ORGANOMETALLICS

ARTICLE

pubs.acs.org/Organometallics

Constructions of 2D-Metallamacrocycles Using Half-Sandwich Ru^{II}_2 Precursors: Synthesis, Molecular Structures, and Self-Selection for a Single Linkage Isomer

Sankarasekaran Shanmugaraju, Arun Kumar Bar, Sachin A. Joshi, Yogesh P. Patil, and Partha Sarathi Mukherjee*

Department of Inorganic and Physical Chemistry, Indian Institute of Science, Bangalore-560 012, India

Supporting Information

ABSTRACT: Coordination-driven self-assembly of oxalato-bridged half-sandwich *p*-cymene ruthenium complex $[Ru_2(\mu\text{-}\eta^4\text{-}C_2O_4)(MeOH)_2(\eta^6\text{-}p\text{-cymene})_2](O_3SCF_3)_2$ (**1a**) with several ditopic donors ($\mathbf{L_a}$−$\mathbf{L_d}$) in methanol affords a series of bi- and tetranuclear metallamacrocycles (**2a** and **3**−**5**). Similarly, the combination of 2,5-dihydroxy-1,4-benzoquinonato (dhbq)-bridged binuclear complex $[Ru_2(\mu\text{-}\eta^4\text{-}C_6H_2O_4)(MeOH)_2(\eta^6\text{-}p\text{-cymene})_2](O_3SCF_3)_2$ (**1b**) with a flexible bidentate amide linker ($\mathbf{L_a}$) in 1:1 molar ratio gave the corresponding tetranuclear complex **2b**. All the macrocycles were isolated as their triflate salts in high yields and were fully characterized by various spectroscopic techniques. Finally, the molecular structures of all the assemblies were determined unambiguously by single-crystal X-diffraction analysis. Interestingly, the combination of acceptor **1a** or **1b** with an unsymmetrical linear ditopic donor $\mathbf{L_a}$ results in a self-sorted linkage isomeric (head-to-tail) macrocycle (**2a** or **2b**) despite the possibility of formation of two different isomeric macrocycles (head-to-head or head-to-tail) due to different connectivity of the donor. Molecular structures of the complexes **2a** and **2b** showed tetranuclear rectangular geometry with dimensions of 5.51 Å × 13.29 Å for **2a** and 7.91 Å × 13.46 Å for **2b**. In both cases, two binuclear Ru^{II}_2 building blocks are connected by a μ-*N*-(4-pyridyl)isonicotinamide donor in a head-to-tail fashion. Surprisingly, the macrocycle **2a** loses one counteranion and cocrystallizes with monodeprotonated 1,3,5-trihydroxybenzene via strong intermolecular π−π stacking and hydrogen bonding. The tweezer complex **3** showed strong fluorescence in solution, and it showed fluorescence sensing toward nitroaromatic compounds. A fluorescence study demonstrated a marked quenching of the initial fluorescence intensity of the macrocycle **3** upon gradual addition of trinitrotoluene and exhibits significant fluorescence quenching response only for nitroaromatic compounds compared to various other aromatic compounds tested.

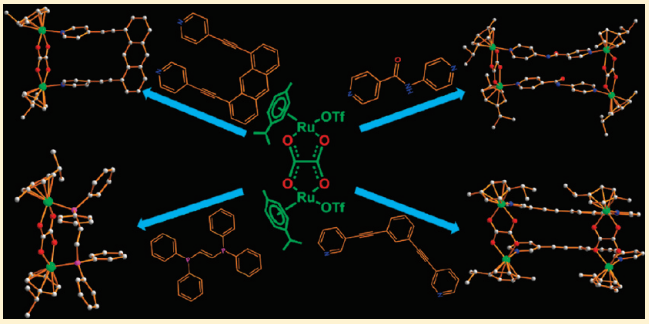

INTRODUCTION

Self-assembly is a process preeminent to the formation of ordered structures emerging spontaneously from the precursors in which the overall structure of the final assemblies is controlled by the symmetry of building blocks.[1] Moreover, it is an omnipresent process throughout nature and allows for various biological functions.[2,3] Synthetic chemists have long been studying and mimicking this natural self-assembly process in the laboratory to understand better nature's own structural diversity and various biological activities.[4] Of the various self-assembly protocols, the metal−ligand directional assembly approach has evolved to be a well-established process for the preparation of supramolecular ensembles with predefined shapes. Various 2D and 3D supramolecular architectures have so far been achieved using a directional bonding approach via self-assembly in the past two decades.[5] Some of these have potential uses in the context of molecular recognition, catalysis, selective guest transportation, and optical materials.[4,5] Platinum(II)- or palladium(II)-based molecular building units are favorites because of the rigid square-planar coordination environment around these metal ions.[6] However, recently organometallic half-sandwich complexes based on Ir, Rh, Os, and Ru fragments are being used as potential building blocks to construct metallacycles and cages due to their stability and interesting electronic as well as structural properties.[7] Such organometallic acceptors have mostly been used with nitrogen-based organic linkers. However, we have recently reported ruthenium−oxygen bond driven self-assembly of an octanuclear incomplete molecular prism.[8] Utilization of supramolecular complexes for certain application depends on the existing functionality, and thus, incorporation of functional groups into the final structure is an efficient way to guide the properties of the resulting molecular architectures. The objective of the current work is to investigate the effect of ligand geometry on the architectural

Received: January 1, 2011
Published: March 07, 2011

nature of the resulting structures. We have selected various ditopic donors of different bite angles, keeping the bite angle of the acceptors constant, to investigate the influence of these donors on the geometry of the resulting architectures.

On the other hand, detection of chemical explosives is a challenging task in the field of chemical sensors, and considerable efforts have been devoted in recent years to the development of suitable chemosensors for detection.[9] Among the various known chemical explosives, trinitrotoluene (TNT) and dinitrotoluene (DNT) are the primary components in many buried landmines, making them a common focus of chemists and materials scientists to design suitable and more efficient sensors for detection.[10] In addition to the known sensor materials such as conjugated organic/inorganic polymers,[11] we have recently shown the possibility of using conjugated metal−organic hybrid discrete assemblies of finite shapes and sizes as fluorescence sensors for nitroaromatic explosives.[12]

Herein, we report the self-assembly of $[Ru_2(\mu\text{-}\eta^4\text{-}C_2O_4)(MeOH)_2(\eta^6\text{-}p\text{-cymene})_2](O_3SCF_3)_2$ (**1a**) or $[Ru_2(\mu\text{-}\eta^4\text{-}C_6H_2O_4)(MeOH)_2(\eta^6\text{-}p\text{-cymene})_2](O_3SCF_3)_2$ (**1b**) with ditopic donors ($\mathbf{L_a}$−$\mathbf{L_d}$) in methanol at room temperature for the formation of two binuclear and three tetranuclear discrete metallamacrocycles of general formula $[Ru_4(\mu\text{-}\eta^4\text{-}C_6H_2O_4$ or $C_2O_4)_2(\mathbf{L_a},\mathbf{L_b})_2(\eta^6\text{-}p\text{-cymene})_4](O_3SCF_3)_4$ (**2a**,**b** and **3**) and $[Ru_2(\mu\text{-}\eta^4\text{-}C_2O_4)(\mathbf{L_c},\mathbf{L_d})(\eta^6\text{-}p\text{-cymene})_2](O_3SCF_3)_2$ (**4**, **5**), respectively in quantitative yields [for **2a** and **2b**, $\mathbf{L_a}$ = *N*-(4-pyridyl)isonicotinamide; for **3**, $\mathbf{L_b}$ = 1,3-bis(3-pyridylethynyl)benzene; for **4**, $\mathbf{L_c}$ = 1,8-bis(4-pyridylethynyl)anthracene; for **5**, $\mathbf{L_d}$ = 1,2-bis(diphenylphosphino)-ethylene] (Scheme 1). The final assemblies were characterized by multinuclear NMR $\{^1H, ^{31}P\}$, IR, and ESI-MS. The molecular structures of all five macrocycles were determined using single-crystal X-ray diffraction analysis of suitable single crystals. The molecular structures of **2a**,**2b** adopt a tetranuclear rectangular geometry with the dimensions 5.51 Å × 13.29 Å for **2a** and 7.91 Å × 13.46 Å for **2b**, whereas macrocycle **3** assumes a tetranuclear tweezer (pincer)-like geometry of dimensions 5.44 Å × 11.37 Å. On the other hand, binuclear supramolecular complexes **4** and **5** adopt rectangular and rhomboidal geometries with the dimensions of 5.53 Å × 11.73 Å for **4** and 5.48 Å × 2.37 Å for **5**, respectively. The tetranuclear tweezer complex **3** was tested as a fluorescence sensor for nitroaromatics (NAC) based on the expectation that an electron-deficient nitroaromatic can encapsulate within the arms of a π-electron-rich pincer via charge-transfer complex formation. Indeed, the solution-state initial fluorescence intensity of **3** was quenched efficiently upon gradual addition of a solution of trinitrotoluene in increased concentration. Interestingly, no such marked quenching was observed upon titrating with other electron-deficient aromatic compounds such as benzoquinone and benzoic acid, which designates that macrocycle **3** can be used as a suitable sensor for nitroaromatic compounds.

Scheme 1. Schematic Representation of the Formation of Tetranuclear (A: 2a,b and B: 3) and Binuclear (C: 4, 5) Macrocycles upon Reactions of Ru^{II}_2-Based Acceptor 1a or 1b with Several Ditopic Donors (L_a−L_d) in Methanol at Room Temperature

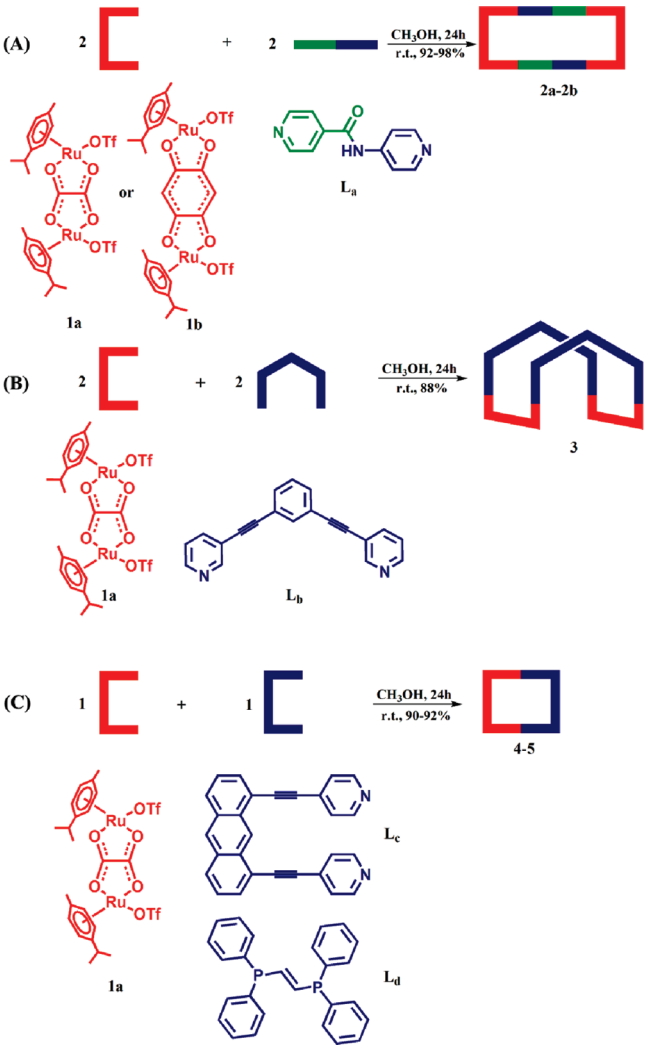

EXPERIMENTAL SECTION

Materials and Methods. The acceptor clips $[Ru_2(\mu\text{-}\eta^4\text{-}C_2O_4)(MeOH)_2(\eta^6\text{-}p\text{-cymene})_2](O_3SCF_3)_2$ (**1a**) and $[Ru_2(\mu\text{-}\eta^4\text{-}C_6H_2O_4)(MeOH)_2(\eta^6\text{-}p\text{-cymene})_2](O_3SCF_3)_2$ (**1b**) were synthesized under a dry nitrogen atmosphere using standard Schlenk techniques following the reported procedures.[13] Solvents were dried and distilled according to standard literature procedures. 1,2-Bis(triphenylphosphino)ethylene ($\mathbf{L_d}$), isonicotinylchloride hydrochloride, 4-aminopyridine, and 1,3-dibromobenzene were purchased from Sigma-Aldrich (USA) and used without further purification. *N*-(4-Pyridyl)isonicotinamide[14] ($\mathbf{L_a}$), 1,3-bis(3-pyridylethynyl)benzene[12b] ($\mathbf{L_b}$), and 1,8-bis(4-pyridylethynyl)-anthracene[15] ($\mathbf{L_c}$) were synthesized following the reported procedures. NMR spectra were recorded on a Bruker 400 MHz spectrometer.

The chemical shifts (δ) in the ^1H NMR spectra are reported in ppm relative to tetramethylsilane (Me_4Si) as internal standard (0.0 ppm) or proton resonance resulting from incomplete deuteration of the NMR solvents: CD_3CN (1.94), CD_3OD (3.33), and $CDCl_3$ (7.26). ^{31}P NMR were recorded at 120 MHz, and the chemical shifts (δ) are reported in ppm relative to external 85% H_3PO_4 at 0.00 ppm. Mass spectral analyses of the self-assembled macrocycles were recorded on an ESI-MS spectrometer using standard spectroscopic grade solvents (CH_3OH or CH_3CN). IR spectra were recorded on a Bruker ALPHA FT-IR spectrometer.

*General Procedure for the Synthesis of Macrocycles **2a**,**b** and **3**−**5**.* To a solid form of the corresponding ditopic donors ($\mathbf{L_a}$−$\mathbf{L_d}$) was added a clear solution of binuclear acceptor clip (**1a** or **1b**) in methanol (2 mL) in 1:1 molar ratio, and the mixture was stirred at room temperature for 24 h in a closed 8 mL glass vial. Immediately, a sharp visual color change

from light yellow to intense yellow for **2a** and **3**−**5** or purple to deep red for **2b** evidenced the progress of the reactions. The solvent was removed under vacuum, and the residue was dissolved in a minimum amount of dichloromethane (DCM) (~2 mL). The diethyl ether was mixed with a concentrated, clear solution to precipitate out the expected macrocycles in pure form.

Macrocycle ***2a***. Acceptor clip **1a** (30 mg, 0.03 mmol) and *N*-(4-pyridyl)isonictinamide $\mathbf{L_a}$ (6.5 mg, 0.03 mmol) were stirred in methanol (4 mL) to obtain **2a**. Isolated yield: 92%. Anal. Calcd for $C_{70}H_{74}F_{12}N_6O_{22}Ru_4S_4$: C, 39.81; H, 3.53; N, 3.98. Found: C, 39.86; H, 3.68; N, 4.23. Melting point > 250 °C. ^{1}H NMR (CD_3CN, 400 MHz): δ 10.24 (s br, 2H, NH-amide), 8.13 (d, 4H, H_α-pyridyl, J = 6.4 Hz), 8.08 (d, 4H, $H_{\alpha'}$-pyridyl, J = 6.8 Hz), 7.64 (d, 4H, H_β-pyridyl, J = 7.2 Hz), 7.56 (d, 4H, $H_{\beta'}$-pyridyl, J = 7.2 Hz), 5.81−5.75 (m, 8H-cymene), 5.66−5.59 (m, 8H-cymene), 2.74 (septet, 4H-C*H*$(CH_3)_2$), 2.11 (s, 12H-C*H*$_3$-cymene), 1.32 (m, 24H-CH(C*H*$_3)_2$). IR (KBr): ν/cm^{-1} 3542.5 (b, NH-amide), 3079.9 (m, C═C of aromatic), 1628.8 (s, C═O-amide and CO-oxalate), 1249.1 (s, C-F of triflate). ESI-MS (m/z): 906.94 [**2a** − $2O_3SCF_3^-$]$^{2+}$, 554.96 [**2a** − $3O_3SCF_3^-$]$^{3+}$, 378.97 [**2a** − $4O_3SCF_3^-$]$^{4+}$.

Macrocycle ***2b***. Acceptor clip **1b** (30 mg, 0.03 mmol) and *N*-(4-pyridyl)isonictinamide $\mathbf{L_a}$ (6.2 mg, 0.03 mmol) were stirred in methanol (4 mL) to obtain **2b**. Isolated yield: 98%. Anal. Calcd for $C_{74}H_{76}F_{12}N_6O_{22}Ru_4S_4$: C, 41.11; H, 3.54; N, 3.89. Found: C, 41.36; H, 3.78; N, 4.23. Melting point >250 °C ^{1}H NMR (CD_3CN, 400 MHz): δ 9.89 (s br, 2H, NH-amide), 8.39 (d, 4H, H_α-pyridyl, J = 6.8 Hz), 8.05 (d, 4H, $H_{\alpha'}$-pyridyl, J = 6.8 Hz), 7.91 (d, 4H, H_β-pyridyl, J = 6.4 Hz), 7.82 (d, 4H, $H_{\beta'}$-pyridyl), 5.86−5.82 (m, 8H-cymene), 5.67−5.60 (m, 8H-cymene), 2.80 (septet, 4H-C*H*$(CH_3)_2$), 2.08 (s, 12H-CH_3-cymene), 1.31 [m, 24H-CH(C*H*$_3)_2$]. IR (KBr): ν/cm^{-1} 3516.8 (b, NH-amide), 3079.8 (m, C═C of aromatic), 1632.6 (s, C═O-amide and CO-quinolate), 1249.1 (s, C-F of triflate). ESI-MS (m/z): 588.35 [**2b** − $3O_3SCF_3^-$]$^{3+}$, 404.01 [**2b** − $4O_3SCF_3^-$]$^{4+}$.

Macrocycle ***3***. Acceptor clip **1a** (10 mg, 0.01 mmol) and 1,3-bis(3-pyridylethynyl)benzene $\mathbf{L_b}$ (3.0 mg, 0.01 mmol) were stirred in methanol (4 mL) for the synthesis of **3**. Isolated yield: 80%. Anal. Calcd for $C_{88}H_{80}F_{12}N_4O_{20}Ru_4S_4$: C, 46.48; H, 3.55; N, 2.46. Found: C, 46.72; H, 3.39; N, 2.62. Melting point > 250 °C. ^{1}H NMR ($CDCl_3$−CD_3OD, 400 MHz): δ 8.05 (s, 4H, H-pyridyl), 7.91 (d, 4H, H-pyridyl, J = 8.0 Hz), 7.84 (m, 4H, H-pyridyl), 7.56 (s, 2H, H-phenyl), 7.34 (m, 4H, H-phenyl), 7.34 (m, 4H, H-phenyl), 7.29 (m, 4H, H-pyridyl), 7.26 (m, 4H, H-pyridyl), 5.81−5.75 (m, 16H-cymene), 2.87 (septet, 4H-CH$(CH_3)_2$), 2.30 (s, 12H-CH_3-cymene), 1.37 (m, 24H-CH$(CH_3)_2$). IR (KBr): ν/cm^{-1} 3079.9 (m, C═C of aromatic), 2231.7 (m, ethynyl), 1626.1(m, CO-oxalate), 1255.6 (s, C-F of triflate). ESI-MS (m/z): 2125.30 [**3** − $O_3SCF_3^-$]$^+$, 988.13 [**3** − $2O_3SCF_3^-$]$^{2+}$.

Macrocycle ***4***. Acceptor clip **1a** (10 mg, 0.01 mmol) and 1,8-bis(4-pyridylethynyl)anthracene $\mathbf{L_c}$ (4.1 mg, 0.01 mmol) were stirred in methanol (4 mL) to obtain **4**. Isolated yield: 90%. Anal. Calcd for $C_{52}H_{44}F_6N_2O_{10}Ru_2S_2$: C, 50.48; H, 3.58; N, 2.26. Found: C, 50.21; H, 3.34; N, 2.43. Melting point > 250 °C. ^{1}H NMR ($CDCl_3$−CD_3OD, 400 MHz): δ 9.23 (s, H-anthracene), 8.68 (s, H-anthracene), 8.23 (d, 4H, H_α-pyridyl, J = 8.4 Hz), 8.18 (d, 2H, H-anthracene, J = 5.6 Hz), 7.87 (d, 4H, H_β-pyridyl, J = 8.4 Hz), 7.59 (m, 4H, H-anthracene), 5.98 (d, 4H-cymene, J = 6.4 Hz), 5.82 (d, 4H-cymene, J = 6.4 Hz), 2.85 (septet, 2H-C*H*$(CH_3)_2$), 2.25 (s, 6H-C*H*$_3$-cymene), 1.36 (d, 12H-C*H*$(CH_3)_2$, J = 6.8 Hz). IR (KBr): ν/cm^{-1} 3059.9 (m, C═C of aromatic), 2211.4 (m, ethynyl), 1636.6 (s, CO-oxalate), 1255.6 (s, C-F of triflate). ESI-MS (m/z): 1087.82 [**4** − $OSO_2CF_3^-$]$^+$, 469.40 [**4** − $2OSO_2CF_3^-$]$^{2+}$.

Macrocycle ***5***. Acceptor clip **1a** (10 mg, 0.01 mmol) and 1,2-bis(triphenylphospheno)ethylene $\mathbf{L_d}$ (3.4 mg, 0.01 mmol) were stirred in methanol (4 mL) to obtain **5**. Isolated yield: 92%. Anal. Calcd for $C_{50}H_{50}F_6O_{10}P_2Ru_2S_2$: C, 47.92; H, 4.02. Found: C, 48.18; H, 4.37. Melting point > 250 °C. ^{1}H NMR (CD_3OD, 400 MHz): δ 7.78−7.29 (m, 20H, phenyl-P*Ph*$_2$), 6.59 (s, 2H-ethylene (dppe)), 5.83 (d, 4H-cymene, J = 6.0 Hz), 5.73 (d, 4H-cymene, J = 6.4 Hz), 2.10 (septet, 2H-C*H*$(CH_3)_2$), 1.98 (s, 6H-CH_3-cymene), 1.15 (d, 12H-C*H*$(CH_3)_2$, J = 6.8 Hz). ^{31}P NMR (CD_3OD, 121 MHz): δ 40.57. IR (KBr): ν/cm^{-1} 3072.5 (m, C═C of aromatic), 1626.1 (s, CO-oxalate), 1275.8 (s, C-F of triflate). ESI-MS (m/z): 1104.21 [**5** − $O_3SCF_3^-$]$^+$, 477.60 [**5** − $2O_3SCF_3^-$]$^{2+}$.

X-ray Data Collection and Structure Refinements. Crystal data of all the assemblies (**2a,b** and **3**−**5**) were collected on a Bruker SMART APEX CCD diffractometer using the SMART/SAINT software.[16] X-ray quality crystals were mounted on a glass fiber with traces of viscous oil. Intensity data were collected using graphite-monochromated Mo Kα radiation (0.7107 Å) at 150 K. The structures were solved by direct methods using SHELX-97[17] incorporated in WinGX.[18] Empirical absorption corrections were applied with SADABS.[19] All non-hydrogen atoms were refined with anisotropic displacement coefficients. Hydrogen atoms were assigned isotropic displacement coefficients, U(H) = 1.2U(C) or 1.5U(C-methyl), and their coordinates were allowed to ride on their respective carbons. Structures were drawn using either ORTEP-3 for Windows[20] or Diamond or PLATON.[21]

Fluorescence Quenching Titration Study. A 2 mL stock solution (5.0×10^{-7} M) of the macrocycle **3** was placed in a quartz cell of 1 cm width, and quenchers stock solution (1.0×10^{-3} M) was added into it in an incremental fashion. The whole titration experiment was carried out at 298 K, and each titration measurement was repeated at least three times to get concordant values. For all measurements the macrocycle (**3**) was excited at λ_{ex} = 283 nm, and the corresponding emission intensity was monitored from 300 nm. Both excitation and emission slit width were 5 nm. No change in the shape of the emission spectra was noticed except significant gradual quenching of the initial fluorescence intensity of **3** upon titration with electron-deficient nitroaromatics. Analysis of the normalized fluorescence emission intensity (I_0/I) as a function of increasing quenchers concentration ([Q]) was well described by the Stern−Volmer equation: $I_0/I = 1 + K_{SV}[G]$. The Stern−Volmer binding constant was calculated from the slope of the Stern−Volmer plot.

RESULTS AND DISCUSSION

Synthesis and Molecular Structure of the Tetranuclear Macrocycles 2a,b and 3. The binuclear acceptor **1a** was treated separately with flexible amide-based ditopic donor $\mathbf{L_a}$ and rigid donor $\mathbf{L_b}$ in 1:1 molar ratio in methanol at room temperature to obtain [2+2] self-assembled **2a** and **3**, respectively, in high yields (Scheme 1). Similarly, the treatment of binuclear acceptor **1b** with $\mathbf{L_a}$ under the same reaction conditions yielded **2b** (Scheme 1). Upon addition of solid donors into the methanolic solution of the corresponding acceptor, immediate consumption of the suspended solid of donors and sharp color changes from light yellow to intense yellow for **2a** and **3** and purple to reddish-brown for **2b** evidenced the progress of the reactions. The macrocycles are highly soluble in common organic solvents. The IR spectra (Figure S1, Supporting Information) of the macrocycles showed strong bands at 1628.8 cm^{-1} for **2a**, 1632.6 cm^{-1} for **2b**, and 1630.3 cm^{-1} for **3**, corresponding to the symmetrical stretching frequencies (ν_{CO}) of the carbonyl groups of the coordinated bis-bidentate oxalato (for **2a** and **3**) or 2,5-dioxydo-1,4-benzoquinonato bridged (for **2b**) ligands, and these symmetrical stretching frequencies (ν_{CO}) in the macrocycles are slightly shifted to higher energy region as compared to that of the starting acceptors (**1a**, ν_{CO} = 1623.7 cm^{-1}; **1b**, ν_{CO} = 1515.8 cm^{-1}) due to the ligand-to-metal coordination. The ^{1}H NMR spectra showed four peaks in the range δ = 8.13−7.56 for **2a** (Figure S2, Supporting Information) and δ = 8.39−7.82 for

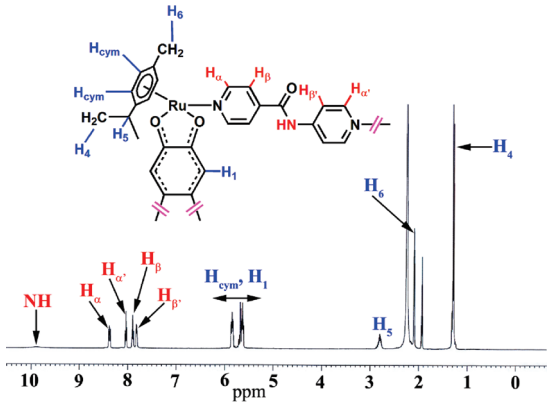

Figure 1. ^{1}H NMR spectra of the macrocycle **2b** recorded in CD_3CN.

2b due to dipyridyl protons of the amide linker ($\mathbf{L_a}$) (Figure 1). Similarly, the resonance corresponding to the pyridyl proton of linker $\mathbf{L_b}$ appeared in the range δ = 8.05−7.84 in the ^{1}H NMR spectra (Figure S3, Supporting Information). All three macrocycles **2a**,**b** and **3** displayed similar signal patterns for the protons of the *p*-cymene ligands (Figure 1 and Figures S2 and S3, Supporting Information). It is worth mentioning that the hydrogen atoms of the pyridine rings of the linkers ($\mathbf{L_a}$, $\mathbf{L_b}$) exhibited a significant downfield shift in all three macrocycles in the ^{1}H NMR spectra due to the loss of electron density upon coordination of the pyridine-N to the Ru(II) centers. However, the ^{1}H NMR spectra did not provide any information about the nuclearity of the final assemblies.

The appearance of prominent peaks in the ESI-MS spectra of the multiply charged ions for **2a** at m/z = 906.94 [**2a** − $2O_3SCF_3^-$]$^{2+}$, 554.96 [**2a** − $3O_3SCF_3^-$]$^{3+}$, 378.97 [**2a** − $4O_3SCF_3^-$]$^{4+}$; for **2b** at m/z = 588.35 [**2b** − $3O_3SCF_3^-$]$^{3+}$, 404.01 [**2b** − $4O_3SCF_3^-$]$^{4+}$; and for **3** at m/z = 2125.30 [**3** − $O_3SCF_3^-$]$^+$, 988.13 [**3** − $2O_3SCF_3^-$]$^{2+}$ indicated the formation of [2+2] self-assembled products. The observed peaks are isotopically resolved and agreed well with their theoretically predicted patterns (Figures S7−S9, Supporting Information). In the case of macrocycles **2a** and **2b**, the formations of two different linkage isomers (head-to-head and head-to-tail) are possible due to the different connectivity of the nonsymmetrical amide linker $\mathbf{L_a}$ (Scheme 2). The appearance of a single peak corresponding to the amide proton and that of a *p*-cymene resonance in the ^{1}H NMR spectra of the rectangles **2a** and **2b** (Figure 1 and Figure S2 in the Supporting Information) indicated the formation of a single linkage isomer over the mixture of isomers. Finally, single-crystal X-ray diffraction analyses of both **2a** and **2b** resolved unambiguously the formation of single linkage isomeric macrocycles in a head-to-tail fashion (Figure 2).

Molecular Structures of 2a and 2b. The molecular structure of **2a** was indirectly determined from the single-crystal X-ray diffraction analysis of **2a**⊃THB. The X-ray diffraction quality single crystals of **2a**⊃THB were obtained by slow vapor diffusion of diethyl ether into a methanolic solution of **2a** along with 1,3,5-trihydroxybenzene (THB) guest. Crystals of **2b** were obtained by slow vapor diffusion of diethyl ether into the solution of **2b** in a methanol/acetone (1:1) solvent mixture. Ball-and-stick views of the macrocycles **2a** and **2b** with the atom numbering are shown in Figure 2. Table 1 presents the crystallographic data and refinement parameters, while selected bond parameters are assembled in Table S1 (Supporting Information). Molecular structures of

Scheme 2. Two Possible Linkage Isomeric Macrocycles for the [2+2] Self-Assembly of 1a or 1b with Ditopic Amide Linker $\mathbf{L_a}$

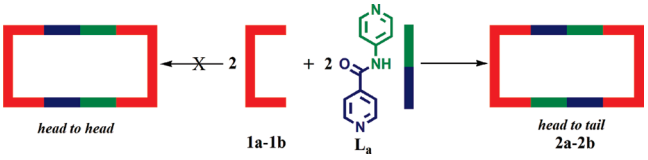

2a and **2b** adopt a similar tetranuclear cationic rectangular geometry composed of [(*p*-cymene)$_4$Ru$_4$(μ-η^4-oxalato)$_2$(μ-*N*-(4-pyridyl)isonicotinamide)$_2$]$^{4+}$(O_3SCF_3)$_4$ (**2a**) and [(*p*-cymene)$_4$Ru$_4$(μ-η^4-dhbq)$_2$(μ-*N*-(4-pyridyl)isonicotinamide)$_2$]$^{4+}$-(O_3SCF_3)$_4$ (**2b**). By assuming that the *p*-cymene occupies three coordination sites, each Ru metal center adopts a three-legged piano-stool conformation, which is a six-coordinated quasi-octahedral geometry. Each Ru center is coordinated to one nitrogen atom of the *N*-(4-pyridyl)isonicotinamide linker and two oxygen atoms from the oxalato (**2a**) or quinonato (**2b**) ligand, resulting in a tetranuclear rectangular geometry with overall dimensions of 5.51 Å × 13.29 Å for **2a** and 7.91 Å × 13.46 Å for **2b**. Interestingly, despite that the amide linker binds to the Ru centers in a head-to-tail fashion in both **2a** and **2b**, the rectangular structures are quite different with respect to the orientation of the amide groups. The carbonyl (−CO−) moieties in the amide groups are directed parallel in **2a** but antiparallel in **2b** (Figure 2). The average Ru−O/N bond distances in **2a** range between 2.097 and 2.115 Å.

Moreover, the two donor molecules in **2a** are not parallel; rather they are squeezed against each other, where the distance between the amide-carbon atoms is 3.746 Å and the two Ru centers of an acceptor unit are separated by 5.510 Å. Interestingly unlike **2a**, the two coordinating amide molecules in **2b** are almost parallel, where the two planes consisting of amide groups are separated by ∼8.2 Å, while the distance between two Ru centers of an acceptor is 7.9 Å. Additionally, the two Ru centers hinged by one donor unit in **2b** are 13.461 Å away from each other, while the distance between two centroids of the bridging quinone molecules is 12.980 Å, indicating that the bridging quinone molecules are slightly squeezed toward each other for the sake of maintaining the piano-stool coordination environment around the Ru metal centers. The average Ru−O/N bond distances in **2b** range between 2.060 and 2.152 Å. The solid-state packing (Figure 2) of both the macrocycles (B; **2a**,**b**) along the *b*-axis shows highly porous rectangular channels. In addition to these structural differences in the skeletons, the mode of crystallization and the solid-state packing pattern of these two macrocycles exhibit huge diversity. Unlike **2b**, **2a** was cocrystallized with 1,3,5-trihydroxybenzene. Moreover, it is surprising to note that one of the OH groups of 1,3,5-trihydroxybenzene is deprotonated, and this monoanionic 1,3,5-trihydroxybenzene replaces one of the triflate anions. The solid-state crystal-packing pattern of **2a** showed that 1,3,5-trihydroxybenzene is stacked between two adjacent aromatic rings (phenyl group of cymene moiety and 4-pyridyl group of 4-aminopyridine moiety) of two neighboring molecules via $\pi-\pi$ stacking interactions (Figure 3). More interestingly though, there are four pyridyl rings in a molecule of **2a**; two pyridyl groups are involved in the aromatic $\pi-\pi$ stacking interactions with the monoanionic guest phluoroglucinol. One of the OH groups of the guest forms H-bonding with the oxygen atom of the neighboring triflate anion, and at the same

dx.doi.org/10.1021/om2000019 |*Organometallics* 2011, 30, 1951–1960

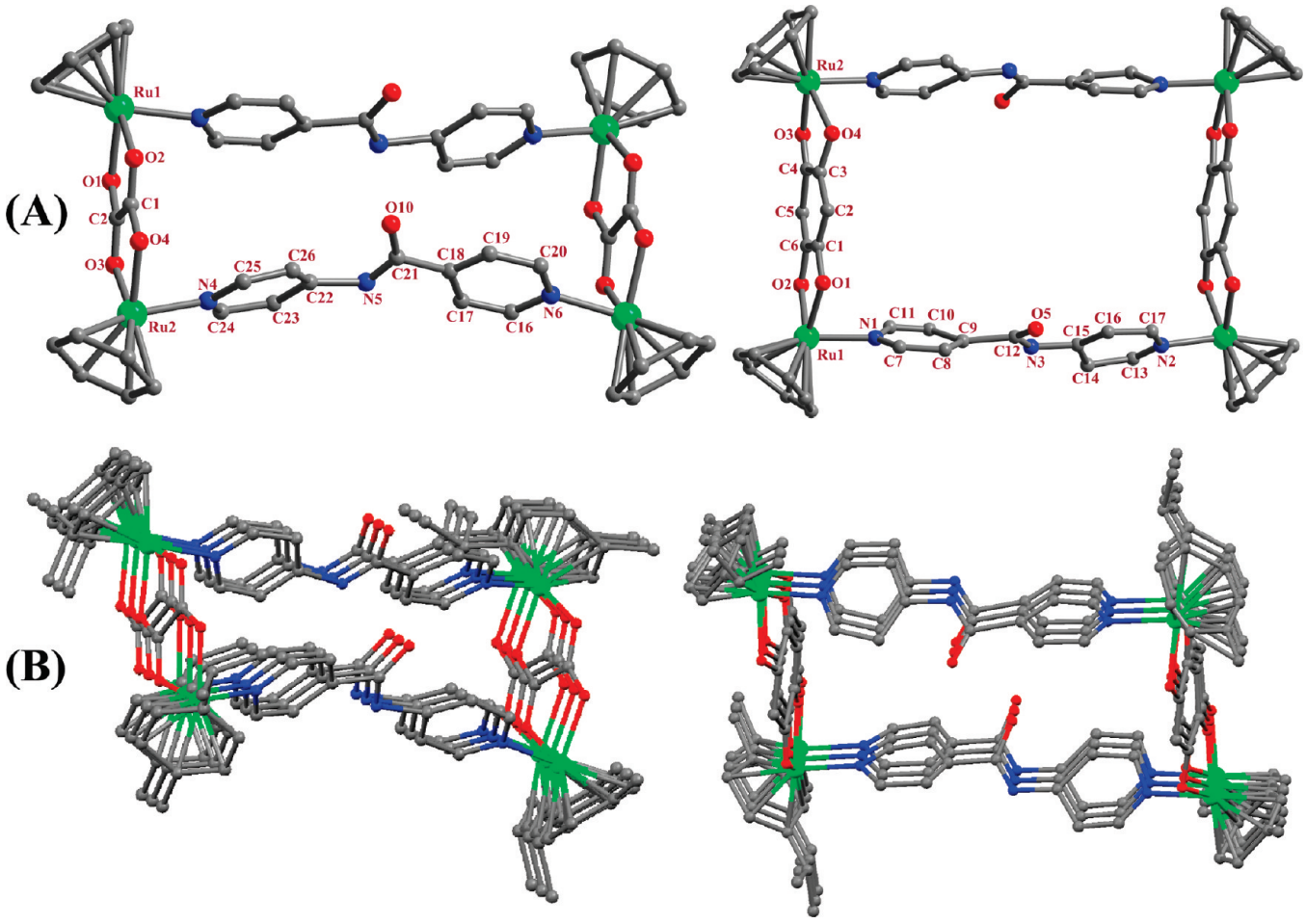

Figure 2. Ball-and-stick representations of the rectangles **2a** (left, A) and **2b** (right, A) with atom numbering and solid-state packing diagrams of **2a** (left, B) and **2b** (right, B) viewed along the crystallographic *b*-axis (color codes: Ru green; O red; N blue; C dark gray). All hydrogen atoms, counteranions, and isopropyl and methyl groups of the *p*-cymene unit are omitted for the sake of clarity.

time the remaining two oxygens of the same triflate anion interact with two other neighboring molecules of **2a** through lone pair$-\pi$ electron interactions. All these interactions result in a 3D supramolecular structure (Figure 3).

Both the macrocycles **2a** and **2b** packed in the solid state along the crystallographic *b*-axis with intermolecular porous channels that are occupied by counteranions (Figure S12−13, Supporting Information).

Molecular Structure of ***3***. Unlike the flexible amide linker $\mathbf{L_a}$, the ditopic donor $\mathbf{L_b}$ is highly rigid due to the presence of a 1,3-diethynylphenyl spacer in between the 3-pyridyl rings. The donor sites in $\mathbf{L_b}$ are projected in the same direction, i.e., parallel with overall geometry resembling the "clip" shape (Scheme 1). The X-ray diffraction quality single crystals of **3** were obtained by slow vapor diffusion of diethyl ether into the methanolic solution of **3** at room temperature. The complex **3** crystallized in the triclinic crystal system with the $P\bar{1}$ space group, having two formula units per unit cell. Crystal structure analysis of **3** revealed that four Ru centers are almost coplanar (dihedral angle = 2.65°) to form a tetranuclear tweezer molecular basal plane with arm lengths 5.462 Å (Ru1−Ru3), 11.374 Å (Ru3−Ru4), 5.443 Å (Ru4−Ru2), and 11.378 Å (Ru2−Ru1). Two *p*-cymene-capped Ru(II) centers Ru1 and Ru3 (or Ru2 and Ru4) are bridged by a μ_2-oxalato bridge to form virtually two nearly coplanar parallel pillars. Ru3 and Ru4 (or Ru1 and Ru2), which are at the ends of longer arms of the rectangular molecular basal plane, are bridged by "clip"-shaped ditopic donor $\mathbf{L_b}$ to form overall tweezer-type architecture **3** (Figure 4). Two bridging "clip" donors ($\mathbf{L_b}$) are situated at the same side of the molecular basal plane, and they are leaning toward each other, presumably to attain the $\pi-\pi$ stacking interactions between two 1,3-diethynylphenyl moieties of the donor ligands. The average Ru−N and Ru−O distances are 2.11 and 2.09 Å, respectively. The solid-state packing diagram of complex **3** along the crystallographic *b*-axis exhibited a strong $\pi-\pi$ stacking interaction between the two adjacent intramolecular 1,3-diethynylphenyl moieties (Figure 4), and the intermolecular porous channels are occupied by triflate counteranions (Figure S14, Supporting Information).

Synthesis and Molecular Structures of Binuclear Macrocycles ***4*** *and* ***5***. As shown in Scheme 1, treatment of a binuclear Ru^{II}_2-based acceptor **1a** with bidentate donors $\mathbf{L_c}$ and $\mathbf{L_d}$ in 1:1 molar ratio in methanol at room temperature affords two different binuclear complexes, **4** and **5**, in good yields, respectively. The formation of binuclear supramolecular architectures was initially characterized by multinuclear (^{1}H and ^{31}P) NMR and ESI-MS spectrometric analyses. The ^{31}P NMR spectrum of **5** showed a single peak at δ = 40.57 ppm, which is highly downfield shifted with respect to the starting donor linker $\mathbf{L_d}$ by 48.10 ppm, and this downfield shift of the phosphorus donor indicated coordination of phosphorus to the ruthenium metal centers (Figure S6,

dx.doi.org/10.1021/om2000019 |*Organometallics* 2011, 30, 1951–1960

Table 1. Crystallographic Data and Refinement Parameters for 2a,b and 3−5

	2a⊃THB	2b	3	4	5
formula	$C_{75}H_{77}F_9N_6O_{22}Ru_4S_3$	$C_{78}H_{78}F_{12}N_6O_{22}Ru_4S_4$	$C_{88}H_{80}F_{12}N_4O_{20}Ru_4S_4$	$C_{104}H_{84}F_{12}N_4O_{23}Ru_4S_4$	$C_{50}H_{48}F_6O_{10}P_2Ru_2S_2$
fw	2085.9	2212.0	2274.1	2518.3	1251.1
cryst syst	triclinic	triclinic	triclinic	triclinic	monoclinic
space group	$P\bar{1}$	$P\bar{1}$	$P\bar{1}$	$P\bar{1}$	$C\,1c\,1$
T, K	150	150	150	150	150
λ(Mo Kα), Å	0.71073	0.71073	0.71073	0.71073	0.71073
a, Å	16.000(4)	9.4273(8)	16.364(13)	18.270(3)	17.0531(6)
b, Å	17.277(4)	10.4518(9)	17.356(15)	18.499(3)	19.1709(7)
c, Å	18.620(4)	22.7684(19)	18.862(15)	19.008(3)	18.1415(7)
α, deg	100.894(4)	87.064(6)	77.887(14)	107.572(3)	90
β, deg	98.465(4)	85.341(6)	75.908(13)	114.973(4)	117.5460(10)
γ, deg	111.165(4)	79.643(6)	86.388(13)	90.672(4)	90
V, Å^3	4581.2(17)	2198.0(3)	5080(7)	5479.4(17)	5258.55
Z	2	2	7	3	2
ρ_{calcd}, g cm^{-1}	1.531	0.841	1.475	1.743	1.273
μ, mm^{-1}	0.829	0.434	0.665	1.027	0.774
GOF[a]	1.041	0.972	0.931	1.305	0.953
R1[b] [$I > 2\sigma(I)$]	0.1055	0.0843	0.1353	0.2370	0.0483
wR2[c] [$I > 2\sigma(I)$]	0.2639	0.2026	0.3119	0.4093	0.1306

[a] GOF = $\{\Sigma[w(F_o^2 - F_c^2)^2]/(n-p)\}^{1/2}$, where n and p denote the number of data points and the number of parameters, respectively. [b] R1 = $(\Sigma||F_o| - |F_c||)/\Sigma|F_o|$. [c] wR2 = $\{\Sigma[w(F_o^2 - F_c^2)^2]/\Sigma[w(F_o^2)^2]\}^{1/2}$, where $w = 1/[\sigma^2(F_o^2) + (aP)^2 + (bP)]$ and $P = [\max(0,F_o^2) + 2F_c^2]/3$.

Supporting Information). ^{1}H NMR spectra of the macrocycles **4** and **5** showed the expected peaks in the aromatic region corresponding to the ditopic donors ($\mathbf{L_c}$,$\mathbf{L_d}$), and the proton of the 4-pyridyl ring of ditopic donor $\mathbf{L_c}$ exhibited a significant downfield shift, attributed to the ligand−metal coordination (Figures S4, S5, Supporting Information).

Overall, NMR analysis supported the formation of a single and symmetrical product in both cases. In the IR spectra of both the assemblies, a sharp peak at 1636.6 cm^{-1} for **4** and 1626.1 cm^{-1} for **5** indicated the presence of coordinated oxalato ligands in the final macrocycles (Figure S1, Supporting Information). The formation of [1+1] self-assembled macrocycles (**4**, **5**) was proved by ESI-MS spectrometric analysis by the appearance of multiply charged molecular ions corresponding to the macrocycles. The multiply charged molecular ions for **4** at m/z = 1087.82 [**4** − $O_3SCF_3^-$]$^+$, 469.40 [**4** − $2O_3SCF_3^-$]$^{2+}$ and for **5** at 1104.21 [**5** − $O_3SCF_3^-$]$^+$, 477.60 [**5** − $2O_3SCF_3^-$]$^{2+}$ were observed in the mass spectra, and these signals are isotopically resolved and matched well with theoretically predicted patterns (Figures S10, S11, Supporting Information).

The molecular structures of binuclear metallamacrocycles [(*p*-cymene)$_2$Ru$_2$(μ-η^4-oxalato)($\mathbf{L_c}$)]$^{2+}$($O_3SCF_3^-$)$_2$ (**4**) and [(*p*-cymene)$_2$Ru$_2$(μ-η^4-oxalato)($\mathbf{L_d}$)]$^{2+}$($O_3SCF_3^-$)$_2$ (**5**) have been determined by single-crystal X-ray diffraction analysis. Perspective drawings of the macrocycles **4** and **5** are given in Figure 5, and selected bond parameters are summarized in Table S3 (Supporting Information). The molecular structure of **4** showed a binuclear rectangular geometry with dimensions of 5.51 Å × 11.56 Å. Each Ru^{II} center is bonded to a *p*-cymene ligand, which is bridged by the dianionic oxalato ($C_2O_4^{2-}$) ligand through its four oxygen atoms and connected to one nitrogen atom of the linker $\mathbf{L_c}$ to adopt a pseudo-octahedral geometry around each metal center. The oxalato ligand connects to two ruthenium metals through four oxygen atoms. The average Ru−N and Ru−O bond distances are 2.138 and 2.113 Å, respectively. As shown in Figure S15 (Supporting Information), the solid-state packing of the binuclear rectangular complex **4** via the crystallographic *a*-axis results in highly porous rectangular channels due to the $\pi-\pi$ interactions between the adjacent molecules. The triflate ($O_3SCF_3^-$) counteranions are located outside the porous channel (Figure S15, Supporting Information).

One can expect the formation of a tetranuclear rectangular complex upon reaction of a binuclear clip-type acceptor (**1a**) and 180° linear ditopic phosphorus donor $\mathbf{L_d}$ via [2+2] self-assembly (Scheme 3). Instead, the exclusive self-sorting of the rhomboidal-like binuclear macrocycle **5** is surprising. The reason for the observed binuclear complex **5** over the molecular rectangle might be the steric hindrance caused by the bulky phenyl substituent on donor atoms with a *p*-cymene cap (Scheme 3) as well as sp^3 hybridization of the phosphorus, which makes the donor semiflexible.

The ball-and-stick representation of the molecular structure of **5** is shown in Figure 5, while selected bond parameters are summarized in Table S3 (Supporting Information). Each ruthenium center is capped with a *p*-cymene molecule and one phosphorus atom of linker $\mathbf{L_d}$ and bridged by a dianionic oxalato ($C_2O_4^{2-}$) ligand. By assuming that the *p*-cymene ligand acts as a three-coordinated ligand, each Ru metal center forms a piano-stool-like quasi-octahedral geometry with dimensions of 2.37 Å × 4.47 Å. The average Ru−P and Ru−O bond distances are 2.375 and 2.115 Å, respectively.

Detection of Nitroaromatics by Fluorescence Quenching. Fluorescence quenching-based detection of chemical explosives is considered one of the most effective and efficient tools for sensing owing to their high sensitivity, easy visualization, and short response time for detection. Nitroaromatic explosives are electron deficient in nature, and the substitution of electron-withdrawing nitro groups on the aromatic rings lowers the energy

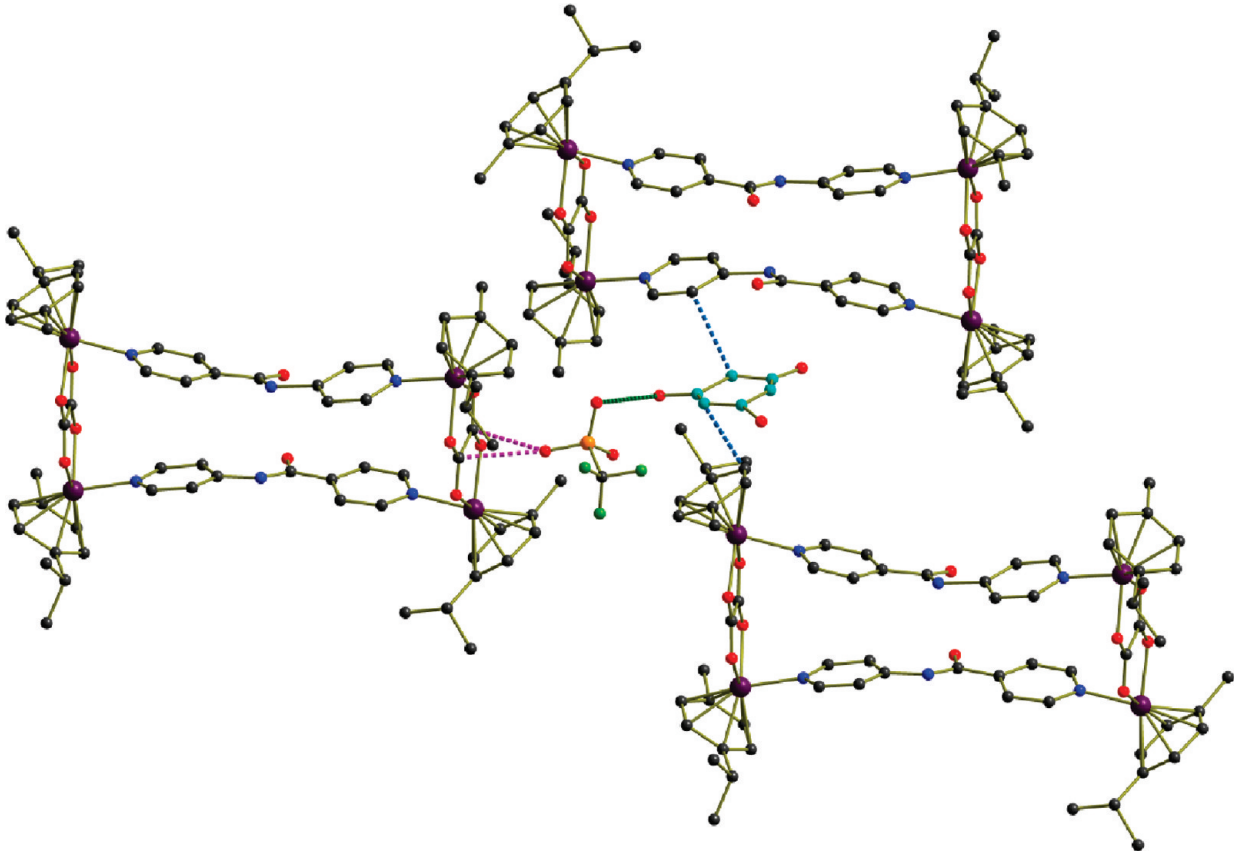

Figure 3. Solid-state packing of host−guest complex **2a**⊃THB (color code: Ru purple; O red; N blue; C dark gray; C-THB cyan).

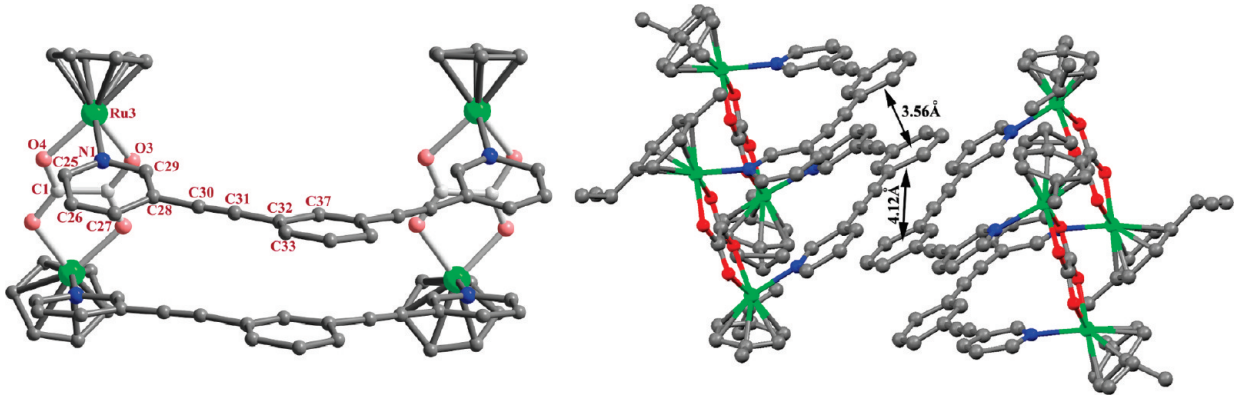

Figure 4. Ball-and-stick representation of tetranuclear tweezer-like macrocycle **3** with atom numbering (left) and the view of the inter/intramolecular Ph−Ph distance (Ru green; O red; N blue; C dark gray). All hydrogen atoms, counteranions, and isopropyl and methyl groups of the *p*-cymene unit are omitted for the sake of clarity.

of the π^* orbital, thereby making them good acceptors. The electronic absorption spectra of macrocycle **3** acquired in methanol solution (5.0×10^{-7} M) was characterized by an intense high-energy band centered at 283 nm and broad low-energy band at around ~380 nm, which are assigned to an intra/intermolecular $\pi-\pi^*$ transition and metal-to-ligand charge-transfer transition, respectively (Figure S16, Supporting Information). Macrocycle **3** exhibits sharp fluorescence emission in methanol solution (5.0×10^{-7} M) at λ = 338 nm upon exciting at λ = 283 nm. Capped *p*-cymene moieties on each ruthenium metal centers help to avoid the intermolecular $\pi-\pi$ stacking between two adjacent macrocycles and thus prevent the chance of self-quenching of initial fluorescence intensity in solution (Figure S17, Supporting Information). To demonstrate the ability of macrocycle **3** to sense electron-deficient nitroaromatic explosives, we performed the titration of **3** with 2,4,6-trinitrotoluene in methanolic solution. Titration of a 5.0×10^{-7} M methanolic solution of **3** with a 1.0×10^{-3} M methanolic solution of TNT showed a gradual quenching of the initial fluorescence intensity (Figure 6). The reason for the observed fluorescence quenching may be due to formation of a charge-transfer complex between π-electron-rich macrocycle **3** (donor) and electron-deficient

dx.doi.org/10.1021/om2000019 |*Organometallics* 2011, 30, 1951–1960

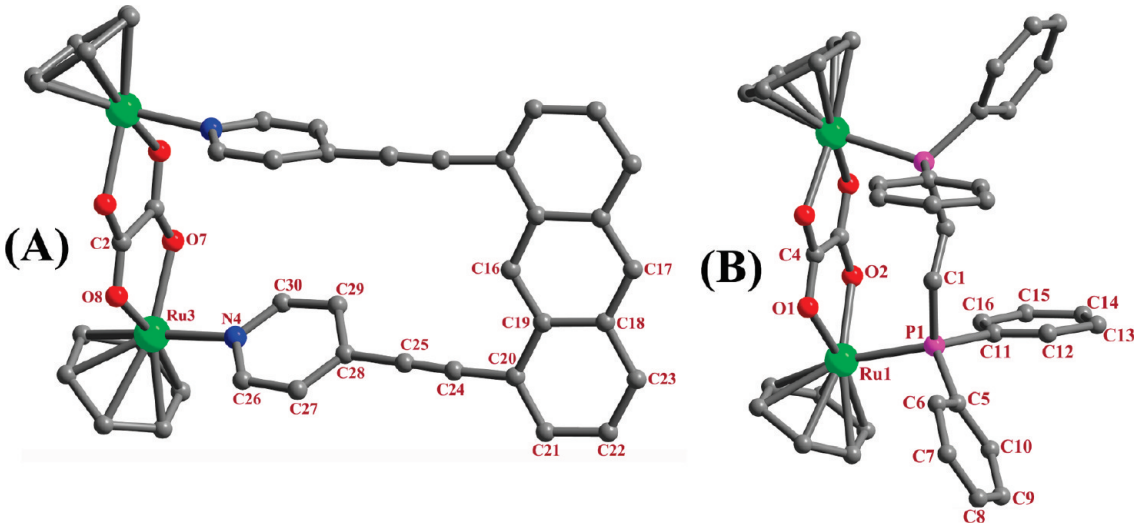

Figure 5. Ball-and-stick representations of binuclear rectangular macrocycles (A) **4** and (B) **5** with atom-numbering scheme. Color code: Ru green; O red; N blue; C dark gray. All the hydrogen atoms, counteranions, and isopropyl and methyl groups of the *p*-cymene unit are omitted for the sake of clarity.

Scheme 3. Schematic Representation of the Formation of [1+1] Self-Sorted Rhomboidal Complex over [2+2] Molecular Rectangle upon Reaction of Binuclear Clip-Type Acceptor 1a and Linear Ditopic Donor L_d

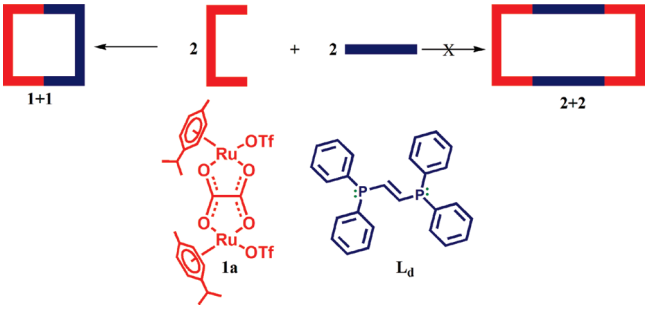

nitroaromatic quenchers (acceptors). Analysis of the normalized fluorescence intensity (I_0/I) as a function of TNT concentration [Q] was carried out by the Stern−Volmer equation: $I_0/I = 1 + K_{SV}[Q]$. The Stern−Volmer binding constant $K_{SV} = 3.3 \times 10^3$ M^{-1} was obtained from the slope of the linear Stern−Volmer plot (Figure 6).

We have also investigated the selectivity of **3** for nitroaromatic compounds over other electron-deficient aromatic systems such as benzoic acid (BA), 4-methoxybenzoic acid (4-MeO-BA), and benzoquinone (BQ). The obtained results (Figure 7) indicate that macrocycle **3** has a quenching response only for nitroaromatic analytes over other aromatic compounds tested due to their low reduction potential value compared to nitroaromatics. This observation is fully consistent with the proposed quenching mechanism in which the electron-deficient nitroaromatics act as a fluorescence quencher (electron acceptor) to electron-rich fluorophores (electron donor) as the result of excited-state charge-transfer complex formation. Surprisingly, though benzoquinone is electron deficient like other aromatic systems tested, significant enhancement in the initial fluorescence intensity was noticed upon titrating with macrocycle **3**. The cause for the observed fluorescence enhancement is probably due to the fact that benzoquinone undergoes transformation to hydroquinone in

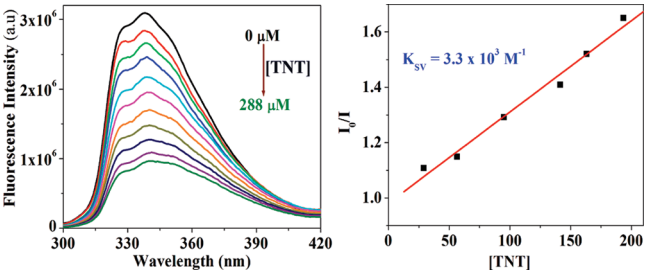

Figure 6. Quenching of initial fluorescence intensity of **3** (left) upon gradual addition of 2,4,6-trinitrotoluene (TNT) in methanol at room temperature and its corresponding Stern−Volmer plot (right).

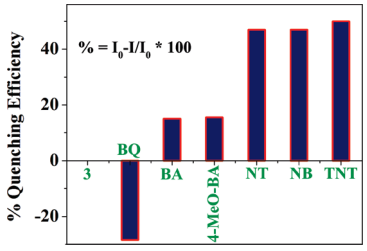

Figure 7. Reduction in fluorescence intensity of macrocycle **3** (plotted as quenching efficiency) observed upon the addition of various analytes. BQ = benzoquinone, 4-MeOBA = 4-methoxybenzoic acid, BA = benzoic acid, NT = nitrotoluene, NB = nitrobenzene, TNT = 2,4,6-trinitrotoluene.

methanolic solution and in turn binds via hydrogen-bonding interaction with the coordinated oxygen of oxalate ($C_2O_4^{2-}$) in **3** rather than the expected charge-transfer complex formation.

CONCLUSIONS

In conclusion, we have synthesized five new complexes, **2a**,**b** and **3**−**5**, via metal ligand coordination-driven self-assembly of half-sandwich *p*-cymene-capped Ru(II)-based binuclear "clip"-type acceptors and a series of various ditopic donors. All five macrocycles are fully characterized by multinuclear (^{31}P and ^{1}H)

dx.doi.org/10.1021/om2000019 |*Organometallics* 2011, 30, 1951–1960

NMR, IR, and ESI-MS spectroscopic studies, and their molecular structures were unambiguously proved by single-crystal X-ray diffraction studies. Despite the possibility of two linkage isomers, exclusive formation of a single linkage isomeric [2+2] self-sorted rectangular architecture **2a**,**b** is quite interesting. Though a "clip"-type donor $\mathbf{L_b}$ resulted in a [2+2] self-sorted tetranuclear metallacycle **3** upon treatment with a binuclear acceptor **1a** in 1:1 molar ratio, [1+1] assembled binuclear molecular complex **4** resulted from the self-assembly of the "clip"-shaped donor $\mathbf{L_c}$ and the same acceptor **1a**. Such difference in topologies of the final architectures can be attributed to the distance between the ligating sites of the donors. The distance between the donor nitrogens in $\mathbf{L_c}$ fits well with the distance between the unsaturated coordination sites of the Ru(II)-based binuclear acceptor **1a** and thereby affords the entropically favored [1+1] self-assembled macrocycle **4**. Moreover, strong $\pi-\pi$ stacking interactions between the two adjacent intramolecular 1,3-diethynylphenyl moieties in the solid-state packing diagram of complex **3** motivated us to check the possibility of this tetranuclear complex to act as a fluorescence sensor for electron-deficient nitroaromatic explosives. Indeed, a significant quenching in the initial fluorescence intensity of **3** was noticed upon titrating with electron-deficient trinitrotoluene, and marked quenching efficiency was observed only for nitroaromatic compounds.

■ ASSOCIATED CONTENT

Supporting Information. IR, NMR, and ESI-MS spectra of macrocycles **2a**,**b** and **3**−**5** including crystallographic details of all the assemblies in CIF format. The solid-state packing diagram of macrocycles **2a**,**b**, **3**, and **4** are available. This material is available free of charge via the Internet at http://pubs.acs.org.

■ AUTHOR INFORMATION

Corresponding Author

*Fax: 91-80-2360-1552. Tel: 91-80-2293-3352. E-mail: psm@ipc.iisc.ernet.in.

■ ACKNOWLEDGMENT

S.S. and Y.P.P. gratefully acknowlege the Council of Scientific and Industrial Research, New Delhi, India, for the award of a research fellowship. P.S.M. and S.A.J. thank the Department of Science and Technology (DST), India, for the financial support. The authors are grateful to Johnson Matthey Pvt. Ltd. U.K. for supplying $RuCl_3$.

■ REFERENCES

(1) (a) Lehn, J.-M. *Supramolecular Chemistry—Concepts and Perspectives*; Wiley-VCH: Weinheim, 1995. (b) Philp, D.; Stoddart, J. F. *Angew. Chem., Int. Ed. Engl.* **1996**, *35*, 1154. (c) Lehn, J.-M. *Proc. Natl. Acad. Sci. U. S. A.* **2002**, *99*, 4763. (d) Whitesides, G. M.; Boncheva, M. *Proc. Natl. Acad. Sci. U. S. A.* **2002**, *99*, 4769. (e) Hof, F., Jr. *Proc. Natl. Acad. Sci. U. S. A.* **2002**, *99*, 4775.

(2) (a) Lehn, J.-M. *Chem. Soc. Rev.* **2007**, *36*, 151.(b) Steed, J. W.; Turner, D. R.; Wallace, K. J. In *Core Concepts in Supramolecular Chemistry and Nano-chemistry*; Wiley: Chichester, U.K., 2007.

(3) (a) Cann, A. J. *Principles of Molecular Virology*; Academic Press: San Diego, 1993. (b) Uchida, M.; Klem, M. T.; Allen, M.; Suci, P.; Flenniken, M.; Gillitzer, E.; Varpness, Z.; Liepold, L. O.; Young, M.; Douglas, T. *Adv. Mater.* **2007**, *19*, 1025.

(4) (a) Whitesides, G.; Grzybowski, B. *Science* **2002**, *295*, 2418. (b) Stang, P. J.; Olenyuk, B. *Acc. Chem. Res.* **1997**, *30*, 502. (c) Leininger, S.; Olenyuk, B.; Stang, P. J. *Chem. Rev.* **2000**, *100*, 853. (d) Holliday, B. J.; Mirkin, C. A. *Angew. Chem., Int. Ed.* **2001**, *40*, 2022. (e) Seidel, S. R.; Stang, P. J. *Acc. Chem. Res.* **2002**, *35*, 972. (f) Fujita, M.; Tominaga, M.; Hori, A.; Therrien, B. *Acc. Chem. Res.* **2005**, *38*, 369. (g) Oliver, C. G.; Ulman, P. A.; Wiester, M. J.; Mirkin, C. A. *Acc. Chem. Res.* **2008**, *41*, 1618. (h) De, S.; Mahata, K.; Schmittel, M. *Chem. Soc. Rev.* **2010**, *39*, 1555. (i) Hu, J.; Ronger, L.; Yip, J. H. K.; Wong, Y. K.; Ma, D. L.; Vittal, J. J. *Organometallics* **2007**, *26*, 6533. (j) Yam, V. W-W.; Tang, R. P.L.; Wong, K. M. C.; Cheung, K. K. *Organometallics* **2001**, *20*, 4476. (k) Das, S.; Bharadwaj, P. K. *Org. Lett.* **2005**, *7*, 1573. (l) Schalley, C. A.; Lutzen, A.; Albrecht, M. *Chem.—Eur. J.* **2004**, *10*, 1072. (m) Toh, N. L.; Nagarithinum, N.; Vittal, J. J. *Angew. Chem., Int. Ed.* **2005**, *44*, 2237.

(5) (a) Zangrando, E.; Casanova, M.; Alessio, E. *Chem. Rev.* **2008**, *108*, 4979. (b) Swiegers, G. F.; Malefetse, T. J. *Coord. Chem. Rev.* **2002**, *225*, 91. (c) Fujita, M. *Chem. Soc. Rev.* **1998**, *27*, 417. (d) Northrop, B. H.; Yang, H.-B.; Stang, P. J. *Chem. Commun.* **2008**, 5896. (e) Cotton, F. A.; Linand, C.; Murillo, C. A. *Acc. Chem. Res.* **2001**, *34*, 759. (f) Li, S.-S.; Northrop, B. H.; Yuan, Q.-H.; Wan, L.-J.; Stang, P. J. *Acc. Chem. Res.* **2009**, *42*, 249. (g) Saalfrank, R. W.; Scheurer, A.; Puchta, R.; Hampel, F.; Maid, H.; Heinemann, F. W. *Angew. Chem., Int. Ed.* **2007**, *46*, 265. (h) Nehete, U. N.; Anantharaman, G.; Chandrasekhar, V.; Murugavel, R.; Roesky, H. W.; Vidovic, D.; Magull, J.; Samwer, K.; Sass, B. J. *Angew. Chem., Int. Ed.* **2004**, *43*, 3832.

(6) (a) Ghosh, S.; Mukherjee, P. S. *Inorg. Chem.* **2009**, *48*, 549. (b) Bar, A. K.; Chakrabarty, R.; Mostafa, G.; Mukherjee, P. S. *Angew Chem., Int. Ed.* **2008**, *47*, 8455. (c) Ghosh, S.; Mukherjee, P. S. *J. Org. Chem.* **2006**, *71*, 8412. (d) Dash, B. P.; Satapathy, R.; Maguire., J. A.; Hosmane, N. S. *Org. Lett.* **2008**, *10*, 2247. (e) Shanmugaraju, S.; Bar, A. K.; Chi, K.-W.; Mukherjee, P. S. *Organometallics* **2010**, *29*, 2971. (f) Ghosh, S.; Turner, D.; Batten, S. R.; Mukherjee, P. S. *Dalton Trans.* **2007**, 1869.

(7) (a) Mattson, J.; Govindaswamy, P.; Furrer, J.; Sei, S.; Yamaguchi, K.; Suss-Fink, G.; Therrien, B. *Organometallics* **2008**, *27*, 4346. (b) Barry, N. P. E.; Therrien, B. *Eur. J. Inorg. Chem.* **2009**, 4695. (c) Therrien, B. *Eur. J. Inorg. Chem.* **2009**, 2445. (d) Therrien, B.; Suss-Fink, G.; Govindaswamy, P.; Renfrew, A. K.; Dyson, P. J. *Angew. Chem., Int. Ed.* **2008**, *47*, 3773. (e) Han, Y.-F.; Lin, Y.-J.; Jia, W.-G.; Weng, L.-H.; Jin, G.-X. *Organometallics* **2007**, *26*, 5848. (f) Han, Y.-F.; Jia, W.-G.; Lin, Y.-J.; Jin, G.-X. *Angew. Chem., Int. Ed.* **2009**, *48*, 6234. (g) Woessner, S. M.; Helms, J. B.; Shen, Y.; Sullivan, B. P. *Inorg. Chem.* **1998**, *37*, 5406. (h) Rajendran, T.; Manimaran, B.; Lee, F.-Y.; Lee, G.-H.; Peng, S.-M.; Wang, C. M.; Lu, K.-L. *Inorg. Chem.* **2000**, *39*, 2016. (i) Yu, W.-B.; Han, Y.-F.; Lin, Y.-J.; Jin, G.-X. *Organometallics* **2010**, *29*, 2827. (j) Wang, J.-Q.; Ren, C.-Y.; Jin, G.-X. *Organometallics* **2006**, *25*, 74. (k) Grote, Z.; Scopelliti, R.; Severin, K. *Eur. J. Inorg. Chem.* **2007**, 694. (l) Lehaire, M.-L.; Scopelliti, R.; Severin, K. *Inorg. Chem.* **2002**, *41*, 5466. (m) Grote, Z.; Scopelliti, R.; Severin, K. *J. Am. Chem. Soc.* **2004**, *126*, 16959. (n) Wang, G.-L.; Yin, Y.-J.; Berke, H.; Jin, G.-X. *Inorg. Chem.* **2010**, *49*, 2193. (o) Jia, A.-Q.; Han, Y.-F.; Jin, Y.-J.; Jin, G.-X. *Organometallics* **2010**, *29*, 232. (p) Govindaswamy, P.; Linder, D.; Lacour, J.; Suss-Fink, G.; Therrien, B. *Chem. Commun.* **2006**, 4691. (q) Han, Y.-F.; Li, H.; Jin, G.-X. *Chem. Commun.* **2010**, 6879. (r) Han, Y.-F.; Jia, W.-G; Yu, W.-B.; Jin, G.-X. *Chem. Soc. Rev.* **2009**, *38*, 3419.

(8) Shanmugaraju, S.; Bar, A. K.; Mukherjee, P. S. *Inorg. Chem.* **2010**, *49*, 10235.

(9) (a) Yinon, J. *Anal. Chem.* **2003**, *75*, 99A–105A. (b) Rouhi, A. M. *Chem. Eng. News* **1997**, *75*, 14. (c) Steinfeld, J. I; Wormhoudt, J. *Annu. Rev. Phys. Chem.* **1998**, *49*, 203.

(10) (a) Maureen, R. A. *C&EN News* **1997**, *March 10*, *14*. (b) Yang, J. S; Swager, T. M. *J. Am. Chem. Soc.* **1998**, *120*, 11864. (c) Jenkins, T. F.; Leggett, D. C.; Miyares, P. H.; Walsh, M. E.; Ranney, T. A.; Cragin, J. H; George, V. *Talanta* **2001**, *54*, 501.

(11) (a) Narayanan, A.; Varnavski, O. P.; Swager, T. M.; Goodson, T., III. *J. Phys. Chem. C* **2008**, *112*, 881. (b) Thomas, S. W., III; Joly, G. D.; Swager, T. M. *Chem. Rev.* **2007**, *107*, 1339. (c) Kim, Y.; Swager, T. M. *Macromolecules* **2006**, *39*, 5177. (d) Thomas, S. W., III; Amara, J. P.; Bjork, R. E.; Swager, T. M. *Chem. Commun.* **2005**, 4572. (e) John,

H.; Sailor, M. J.; Magde, D.; Trogler, W. C. *J. Am. Chem. Soc.* **2003**, *125*, 3821. (f) Toal, S. J.; Sanchez, J. C.; Dugan, R. E.; Trogler, W. C. *J. Forensic Sci.* **2007**, *52*, 79.

(12) (a) Ghosh, S.; Mukherjee, P. S. *Organometallics* **2008**, *27*, 316. (b) Ghosh, S.; Gole, B.; Bar, A. K.; Mukherjee, P. S. *Organometallics* **2009**, *28*, 4288.

(13) (a) Barry, N. P. E.; Therrien, B. *Inorg. Chem. Commun.* **2008**, *11*, 1300. (b) Yan, H.; Suss-Fink, G.; Neels., A.; Stoeckli-Evans, H. *J. Chem. Soc., Dalton Trans.* **1997**, 4345.

(14) Kumar, D. K.; Jose, D. A.; Dastidar, P.; Das, A. *Langmuir* **2004**, *20*, 10413.

(15) Mukherjee, P. S.; Min, K. S.; Ariff, A. M.; Stang, P. J. *Inorg. Chem.* **2004**, *43*, 6345.

(16) *SMART/SAINT*; Bruker AXS, Inc.: Madison, WI, 2004.

(17) Sheldrick, G. M. *SHELX-97, Program for the Solution and Refinement of Crystal Structures*; University of Göttingen: Göttingen, Germany, 1998.

(18) Farrugia, L. J. *WinGX: An Integrated System of Windows Programs for the Solution, Refinement and Analysis for Single Crystal X-ray Diffraction Data*, version 1.65.04; Department of Chemistry: University of Glasgow, 2003 (Farrugia, L. J. *J. Appl. Crystallogr.* **1999**, *32*, 837).

(19) Sheldrick, G. M. *SADABS, Bruker Nonius Area Detector Scaling and Absorption Correction*, version 2.05; University of Göttingen: Göttingen, Germany, 1999.

(20) Farrugia, L. J. *ORTEP-3* for Windows, version 1.08. *J. Appl. Crystallogr.*, **1997**, *30*, 565.

(21) Spek, A. L. *Acta Crystallogr.* **1990**, *A46*, C34.